Hydrodynamic Synchronization of Chiral Microswimmers

Sotiris Samatas and Juho Lintuvuori
Univ. Bordeaux, CNRS, LOMA, UMR 5798, F-33400 Talence, France

(Received 24 June 2022; revised 15 November 2022; accepted 19 December 2022; published 9 January 2023)

We study synchronization in bulk suspensions of spherical microswimmers with chiral trajectories using large scale numerics. The model is generic. It corresponds to the lowest order solution of a general model for self-propulsion at low Reynolds numbers, consisting of a nonaxisymmetric rotating source dipole. We show that both purely circular and helical swimmers can spontaneously synchronize their rotation. The synchronized state corresponds to velocity alignment with high orientational order in both the polar and azimuthal directions. Finally, we consider a racemic mixture of helical swimmers where intraspecies synchronization is observed while the system remains as a spatially uniform fluid. Our results demonstrate hydrodynamic synchronization as a natural collective phenomenon for microswimmers with chiral trajectories.

DOI: 10.1103/PhysRevLett.130.024001

Introduction.—Microswimmers are a subset of active matter systems and correspond to microscopic elements self-propelling within a fluid environment. Natural microswimmers consist of biological microorganisms [1–3] and their collective dynamics has gained a lot of interest of late [4–12]. This has inspired research on synthetic microswimmers, typically based on phoretic Janus particles [13–15]. The interest for developing artificial swimmers has been fueled by the various promising possibilities for applications such as microcargo transportation [16–19], targeted drug delivery [19–22], artificial insemination [19,23], and microsurgery [19,20,24–26].

Most theoretical studies of microswimmer suspensions have concentrated on particles that swim in straight lines, with simulations predicting the spontaneous formation of collective swimming along a common direction—uniform polar order [27–33]. However, microorganisms typically have intrinsic chirality and tend to swim along helical paths [34–44]. Similarly, any asymmetry due to imperfections in the shape of the colloids or in their catalytic coating would also lead to chiral motion for artificial swimmers [13,45–48].

Continuum descriptions based on the long-range hydrodynamics produced by flow singularities [49–52] have been extensively used in the past, with some works including chiral flows [53–55]. However, these models fail to capture near-field hydrodynamic effects, which are believed to be crucial for the formation of polar order [29,30].

Most of the current theoretical work of active particles moving along chiral paths relies on dry microscopic descriptions such as active Brownian particle (ABP) models [56–65]. These effectively account for excluded volume effects, but neglect hydrodynamic interactions. Simulations of rotational dry models have predicted large-scale synchronization, when a Kuramoto-type alignment term is included [57,66]. Very recently, work on the hydrodynamics of chiral swimmers has started to emerge, but has so far been limited to single and two particle systems [67–72].

Explicitly incorporating chirality in hydrodynamic models used to study microswimmer suspensions could have an important effect regarding the emergence of collective states, such as large-scale collective oscillations [73,74], polar order [27–33] or hydrodynamic synchronization [75–81]. While synchronization arising from active flows has been predicted for linear trimers [75] and for rotors on a two-dimensional lattice [79], the ability of microswimmers to spontaneously synchronize (or not) in freely moving bulk suspensions, remains an open question.

Here, we show that swimmers with chiral trajectories can synchronize their rotation in a fully three-dimensional suspension. We consider finite sized swimmers, with a surface slip-flow arising from the general solution for self-propulsion at low Reynolds numbers [82], corresponding to a rotating source dipole flow inclined at an angle ψ with respect to the particle polar direction. A synchronized state, corresponds to the alignment of these dipoles. We study three distinct cases: circular swimmers, helical swimmers, and a racemic mixture of left-handed and right-handed helical swimmers. In all cases, the spontaneous formation of synchronized states is observed.

Model for rotational squirmers.—To model the microswimmers, we consider spherical particles of radius a, and extend the standard squirmer model [83,84] to include rotational slip flows. Based on Lamb's general solution, the tangential slip flow at the particle surface is given in spherical coordinates by an infinite series of modes for the polar and azimuthal components $\mathbf{e}_\theta$ and $\mathbf{e}_\varphi$ [82]. The lowest order modes correspond to self-propulsion (source dipoles

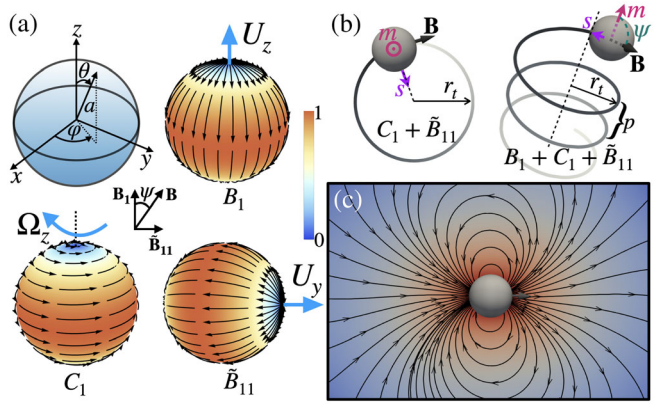

FIG. 1. Model for rotational squirmers. (a) The surface slip flows corresponding to the different modes: B_1, C_1, and $\tilde{B}_{11}$ in the particle frame. The magnitude of the normalized surface velocity (slip flow) for each mode is represented by a color-code and the streamlines are colored black. (b) The particle trajectories in the lab frame, corresponding to circular (left) and helical (right) swimming. The unit vectors $\boldsymbol{m}$ and $\boldsymbol{s}$ correspond to the particle polar and azimuthal axes, respectively, and ψ is the inclination angle with respect to $\boldsymbol{m}$. (c) Swimmer flow field obtained from the simulations, corresponding to a source dipole $\mathbf{B}$ (neutral squirmer). The magnitude of the fluid velocity is coloured using a logarithmic scale and overlaid by black streamlines.

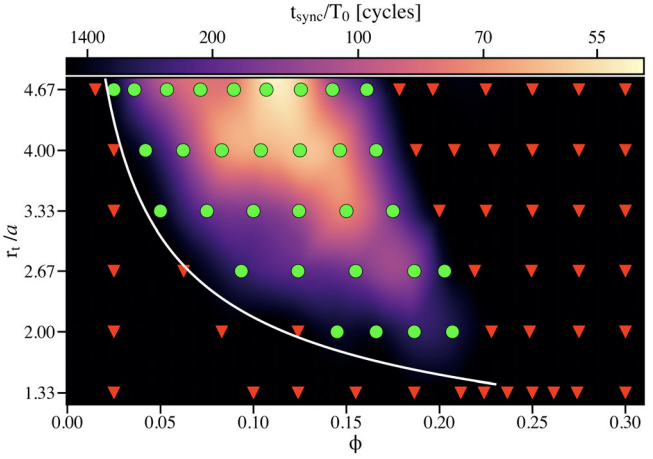

FIG. 2. Synchronization diagram for circular swimmers ($\psi = 90°$) as a function of the volume fraction ϕ and particle trajectory radius r_t. Green circles indicate global synchronization, and the red triangles mark isotropic states. The synchronization region is colored according to a waiting time t_{sync}/T_0 corresponding to the total time elapsed from the start of the simulation until synchronization is reached. The white curve corresponds to $\phi = \phi_c'[(4/3\pi a^3)/2\pi r_t^2 a]$ with $\phi_c' = 70\%$. (see text and Supplemental Material [85] for details).

and rotlets), while the higher order terms correspond to fluid mixing. We choose [82,85]

$$u_\theta|_{r=a} = B_1 \sin\theta + \tilde{B}_{11} \cos\theta \sin\varphi$$
$$u_\varphi|_{r=a} = C_1 \sin\theta + \tilde{B}_{11} \cos\varphi. \quad (1)$$

The B_1 mode corresponds to the source dipole in the standard squirmer model [top right panel in Fig. 1(a)]. C_1 leads to a rotation of the particle around its polar axis $\boldsymbol{z}$ (or $\boldsymbol{m}$) with an angular velocity $\omega_0 = C_1/a$ [bottom left panel in Fig. 1(a)]. $\tilde{B}_{11}$ corresponds to a source dipole along $\boldsymbol{y}$ [bottom right panel in Fig. 1(a)]. The total swimmer flow field corresponds to a single source dipole $\mathbf{B}$ with magnitude $B = \sqrt{\tilde{B}_{11}^2 + B_1^2}$, which rotates around the polar axis ($\boldsymbol{m}$) at an inclination $\psi = |\tan^{-1}(\tilde{B}_{11}/B_1)|$ (Fig. 1). An isolated particle has a swimming speed $v_0 = \frac{2}{3}B$. When $\psi = 90°$ ($B_1 = 0$) the swimmers have circular trajectories in a plane perpendicular to $\boldsymbol{m}$ (left in Fig. 1(b)). The radius of the trajectory is given by $r_t = 2\tilde{B}_{11}a/(3C_1)$ and the period by $T_0 = 2\pi/\omega_0 = 2\pi a/C_1$. For $\psi \neq 90°$ and $\psi \neq 0°$ the trajectories become helical with pitch length $p = 4\pi B_1 a/(3C_1)$ [right panel in Fig. 1(b)]. To characterize the helical swimming, we define the ratio $\lambda \equiv r_t/p = \tilde{B}_{11}/(2\pi B_1)$ [85].

To study the collective dynamics of suspensions of N swimmers, we use the lattice Boltzmann method [85]. The typical particle Reynolds number is $\mathrm{Re} \sim 0.01$ with simulation times ~100 s. (see Supplemental Material [85] for details of simulations and mapping to SI units). An orientationally ordered state, corresponds to the alignment of the source dipoles $\mathbf{B}$. The amount of alignment can be measured by considering a velocity order parameter $P_v(t) = (|\sum_i^N \hat{\boldsymbol{v}}_i|/N)$, where $\hat{\boldsymbol{v}}_i = \boldsymbol{v}_i/v_i$. To further quantify the ordering, we measure the alignment along the azimuthal $\boldsymbol{s}$ and polar $\boldsymbol{m}$ directions, by calculating $P_{s|m}(t) = (|\sum_i^N \boldsymbol{s}_i|\boldsymbol{m}_i|/N)$. $P_{v|s|m} = 1$ corresponds to complete order, and 0 to an isotropic state.

Synchronization of circular swimmers.—Starting from isotropic initial conditions, we find that circular swimmers spontaneously synchronize their rotation when $\phi \approx 3\ldots23\%$ and $r_t \approx 2\ldots5a$ (Fig. 2). The synchronization corresponds to the spontaneous alignment of the particle velocities, with the growth of both azimuthal and polar order, where typically $P_s \approx P_m \approx P_v \gtrsim 0.85$ at long times [Fig. 3(a)]. The phase locking is apparent from the distribution of the lag angle $\alpha = \alpha_{1,2}^{s\perp}$ calculated from all the particle pairs, considering the $\boldsymbol{s}$ vectors of two different rotors in the plane perpendicular to the global polar director, $\boldsymbol{P}_M \sim \sum_i^N \boldsymbol{m}_i$. The distribution of α changes from uniform at $t \approx 0$ to a normal distribution with a peak at $\alpha \approx 0$ in the globally synchronized state [Fig. 3(d)]. In this state, the particle trajectories are circular and aligned perpendicularly to $\boldsymbol{P}_M$ [right in Fig. 3(e)]. The particle positions remain isotropic with the pair-correlation functions $g(r)$, $g(r_\perp)$, and $g(r_{||})$ showing liquidlike structure [Fig. 3(b)].

The likelihood of the synchronization depends on the volume fraction ϕ and the trajectory radius r_t (Fig. 2). At low ϕ the system remains in an isotropic state with the

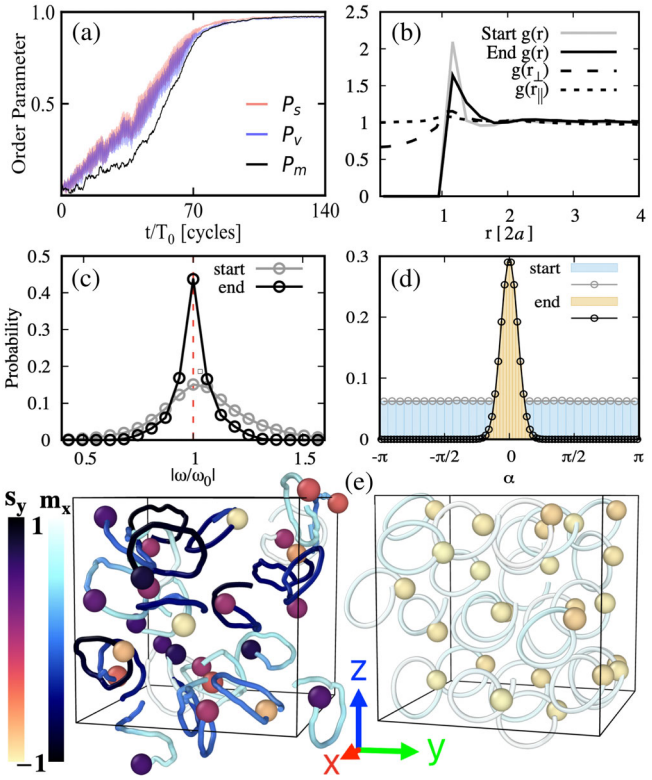

FIG. 3. (a) Circular swimmers: Example of a typical time evolution of the azimuthal P_s (red), velocity P_v (blue), and polar P_m (black) order parameters. (b) Radial distribution function $g(r)$ of the system at the beginning (gray) and at the end (black) of the simulation. The $g(r_\perp)$ ($g(r_{||})$) are calculated perpendicular (parallel) to the polar director $\boldsymbol{P}_M$. Probability distribution of the (c) angular velocities ω and (d) phase lag angle α between all particle pairs, at the start and end of the simulation. (e) Snapshots of 25 selected particles at the beginning (left) and end (right) of the simulation. The particles are colored according to the y component of their $\boldsymbol{s}$ vector. The trajectories are shown over one period and colored according to the x component of the swimmer's $\boldsymbol{m}$ vector. (The data correspond to $\phi \approx 0.15$ and $r_t \approx 3.33a$).

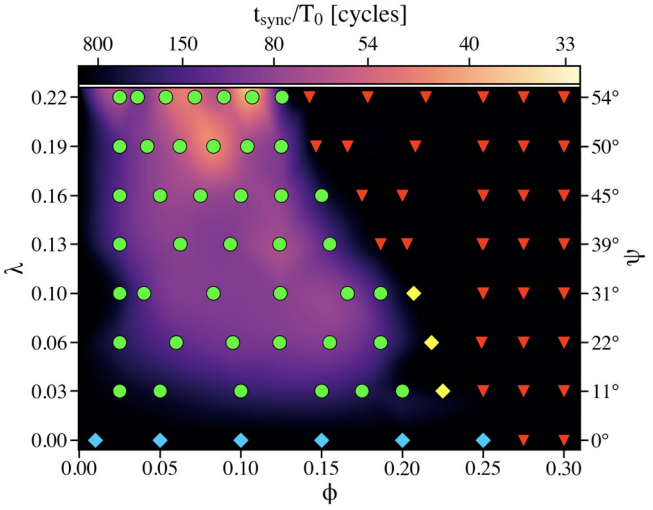

FIG. 4. State diagram for helical swimmers as a function of ϕ and $\lambda = r_t/p$. The green circles correspond to global synchronization, and red triangles to isotropic states. The blue diamonds mark polar order for classic linear neutral squirmers and yellow diamonds correspond to finite polar order in the absence of synchronization for chiral swimmers. (data correspond to $p \approx 21a$).

circular trajectories randomly oriented and distributed. When ϕ is increased, the trajectories become jagged in the isotropic state [left in Fig. 3(e)]. At long times the trajectories align [right in Fig. 3(e)]. The distribution of rotational frequencies ω has a peak at ω_0 and the width likely arises from the hydrodynamic fluctuations [Fig. 3(c)]. Interestingly, the particle dynamics is reminiscent of the active-absorbing state transition predicted for dry circular swimmers in two dimensions (2D) [62]—the diffusive dynamics in the isotropic state becomes subdiffusive when the spontaneous synchronization occurs [85]. However, in the 2D dry system, where the particles interact exclusively via steric collisions, only local synchronization was observed [62]. This suggests that hydrodynamic interactions are crucial for the large scale synchronization observed here.

Previous studies of linear squirmers predict that the alignment of source dipoles corresponding to the formation of uniaxial polar order is dominated by near-field hydrodynamic interactions [29,30]. When $r_t \sim a$, an isolated swimmer sweeps an area $\sim r_t^2$ during one period T_0, and can be thought to occupy an effective volume $2\pi r_t^2 a$. The lower-ϕ limit for the synchronization region, closely corresponds to the random close packing of discotic cylinders with volume $2\pi r_t^2 a$ [85] (white line in Fig. 2). Above this line, the effective volumes overlap in the isotropic state, and the swimmers have a high probability of interacting via near-field hydrodynamics.

To study the ordering dynamics, we measure the total time t_{sync} from the beginning of the simulation until synchronization is reached. The fastest formation is observed in the middle of the synchronized region (Fig. 2). For a given r_t, if ϕ is too large no synchronization is observed. This implies the existence of a dynamic bottleneck where the particles have multiple collisions during their full-rotation time T_0, hindering the growth of global alignment. For simulations towards the high-ϕ end of the synchronization region, t_{sync} is increased (Fig. 2), and the order parameters fluctuate close to zero before the growth of the order begins.

Helical swimmers.—The helical swimmer trajectories are characterized by the ratio between the radius of curvature of the trajectory and the pitch length $\lambda = r_t/p$ [Fig. 1(b)]. The particle motion is three-dimensional, leading to an increase of the probability of near-field interactions. Hence, synchronization is observed at lower ϕ than in the case of pure rotors (Figs. 2 and 4). Similarly to circular swimmers, a high degree of order is observed in the

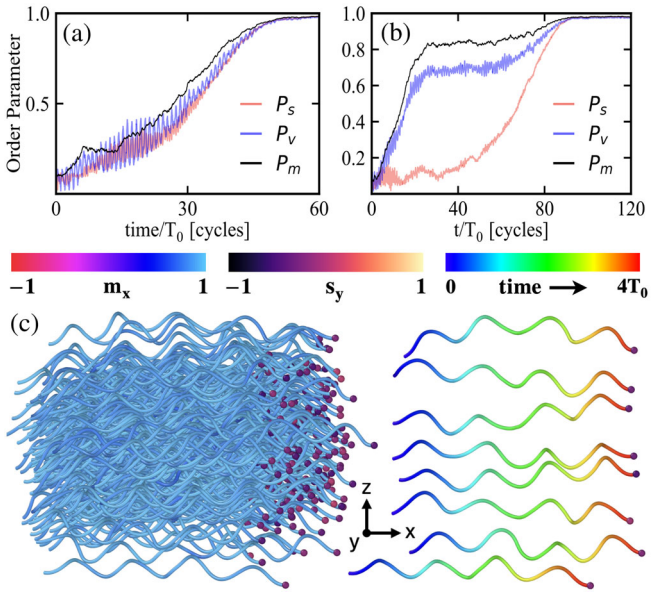

FIG. 5. Helical swimmers: Time evolution of the order parameters P_s (red), P_v (blue), and P_m (black) for (a) $\phi \approx 0.083$, $\lambda \approx 0.19$, and (b) $\phi \approx 0.125$, $\lambda \approx 0.1$. (c) Snapshots of the system in the synchronized state. The uwrapped trajectories of all the $N = 286$ helical swimmers colored according to $\boldsymbol{m}_x$ (left). 8 selected microswimmers with their trajectories colored as a function of time (right). The particles are colored according to $\boldsymbol{s}_y$. [The snapshots in (c) correspond to $\phi \approx 0.15$, $\lambda \approx 0.16$].

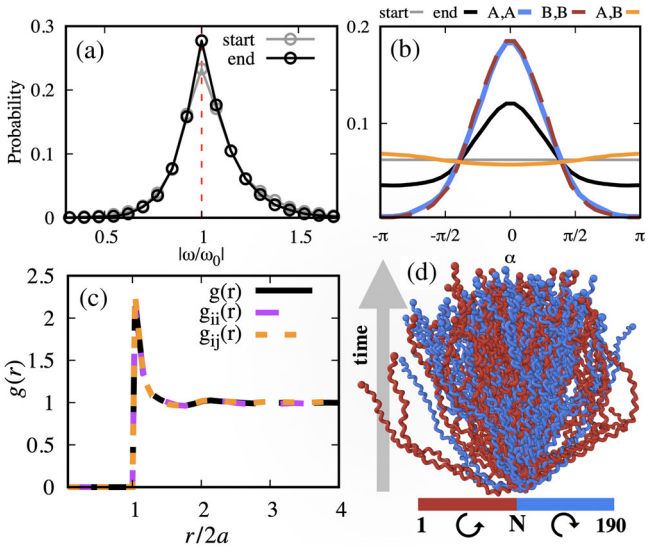

FIG. 6. Racemic mixture: Distributions of the (a) spinning frequency ω and (b) the phase-angle difference α calculated for all swimmer pairs (black), for clockwise (blue) and counterclockwise (red) rotating populations, as well as for the cross population (orange). (c) Total (black), homochiral (violet), and heterochiral (orange) radial distribution functions. (d) Snapshot of the unwrapped trajectories at the steady state after $20T_0$. (The data correspond to $\phi \approx 0.1$ and $\lambda \approx 0.16$).

synchronized state [Figs. 5(a) and 5(b)], and the particles swim along a common direction, with their helical trajectories aligned [Fig. 5(c)]. Interestingly, when the ratio $\tilde{B}_{11}/B_1$ is decreased, the ordering dynamics is observed to change from a smooth growth to a two-step process where the velocity alignment initially corresponds only to alignment in the polar direction [see, e.g., Figs. 5(a) and 5(b), for $\lambda \approx 0.19$ and $\lambda \approx 0.1$, respectively]. Both the rotational frequency and the phase locking show comparable behavior to the circular swimmers [85].

When $\lambda = 0$, the swimmers correspond to achiral neutral squirmers and the formation of pure polar order ($P_m > 0$; $P_s \sim 0$) is observed (blue diamonds in Fig. 4) in agreement with [27–33]. Remarkably, we also find cases with $\lambda > 0$ with stable polar order in the absence of azimuthal ordering ($P_m > 0$; $P_s \approx 0$) (yellow diamonds in Fig. 4).

The synchronization spans to low chiralities, and is observed for $\lambda \approx 0.03 \ldots 0.22$ and $\phi \approx 2.5 \ldots 20\%$ (Fig. 4). The λ range corresponds to experimentally observed trajectories of biological swimmers such as $\lambda = r_t/p \approx 0.05$ for *T. thermophila* [39] and $\lambda \approx 0.15$ for the three-dimensional swimming of sperm [40]. We note that the transition between synchronized chiral states and the linear polar state ($\lambda = 0$) is predicted to occur between $\lambda \lesssim 0.03$ and $\lambda = 0$ (Fig. 4). This suggests that synchronization may well be observable at lower chiralities than $\lambda \approx 0.03$ considered in Fig. 4.

Racemic mixture.—Finally, to study the effect of frustration, we construct a racemic mixture composed of right-handed and left-handed helical swimmers by choosing $C_1 = \pm 0.001$ (Fig. 6). We start from a fully mixed isotropic state. At the steady state, the particles, on average, swim along a common direction [Fig. 6(d)] and the rotational frequency ω is observed to peak at ω_0 [Fig. 6(a)]. The intraspecies α shows strong phase locking [blue and red curves in Fig. 6(b)], whereas for the cross species no significant peak is observed [orange curve Fig. 6(b)], due to the oppositely spinning populations. However, the distribution shows a slight preference for $\alpha = \pm\pi$, which corresponds to a parallel orientation of the in-plane projections of the source dipoles [85]. Within the timescale of the simulations, we observe no spatial separation of the swimmers—the fluidlike pair-correlation function calculated within species and cross species matches with the $g(r)$ of the whole system [Fig. 6(c)].

Conclusions.—Using hydrodynamic simulations we have investigated suspensions of microswimmers with chiral trajectories at the limit of zero thermal noise. The results suggest the emergence of hydrodynamic synchronization as a naturally occurring collective phenomenon for microswimmers. The predictions should be relevant to a wide variety of experimental systems; such as helically swimming bacteria [39] and sperm [40], or chiral Quincke rollers [86] and spherical ciliates [87], where rotational motion occurs naturally. The observation of the intraspecies synchronization in the racemic mixture, provides

a surprising example of two synchronized, interpenetrating, fluids. Further, it demonstrates that the synchronization is maintained in the presence of hydrodynamic fluctuations arising from the source-dipole $1/r^3$ far fields. This suggests that it could be interesting to (re)analyze three-dimensional correlations in the rotational degrees of freedom in systems exhibiting polar order, such as areas of uniform order in bacterial systems [4–12] or polar flocks in motile colloids [88].

Discussions with Zaiyi Shen and Alois Würger are gratefully acknowledged. S. S. acknowledges University of Bordeaux, and the A. G. Leventis Foundation for funding, as well as cluster CURTA at MCIA for computational time. J. S. L. acknowledges the French National Research Agency (ANR) through Contract No. ANR-19-CE06-0012-01 and la region Nouvelle Aquitaine project GASPP for funding.

[1] D. L. Koch and G. Subramanian, Collective hydrodynamics of swimming microorganisms: Living fluids, Annu. Rev. Fluid Mech. **43**, 637 (2011).
[2] E. Lauga, Bacterial hydrodynamics, Annu. Rev. Fluid Mech. **48**, 105 (2016).
[3] E. Lauga, *The Fluid Dynamics of Cell Motility* (Cambridge University Press, Cambridge, England, 2020), Vol. 62.
[4] C. Dombrowski, L. Cisneros, S. Chatkaew, R. E. Goldstein, and J. O. Kessler, Self-Concentration and Large-Scale Coherence in Bacterial Dynamics, Phys. Rev. Lett. **93**, 098103 (2004).
[5] A. Sokolov, I. S. Aranson, J. O. Kessler, and R. E. Goldstein, Concentration Dependence of the Collective Dynamics of Swimming Bacteria, Phys. Rev. Lett. **98**, 158102 (2007).
[6] C. W. Wolgemuth, Collective swimming and the dynamics of bacterial turbulence, Biophys. J. **95**, 1564 (2008).
[7] L. H. Cisneros, R. Cortez, C. Dombrowski, R. E. Goldstein, and J. O. Kessler, Fluid dynamics of self-propelled microorganisms, from individuals to concentrated populations, in *Animal Locomotion* (Springer, New York, 2010), pp. 99–115.
[8] H.-P. Zhang, A. Beer, E.-L. Florin, and H. L. Swinney, Collective motion and density fluctuations in bacterial colonies, Proc. Natl. Acad. Sci. U.S.A. **107**, 13626 (2010).
[9] A. Sokolov and I. S. Aranson, Physical Properties of Collective Motion in Suspensions of Bacteria, Phys. Rev. Lett. **109**, 248109 (2012).
[10] H. H. Wensink, J. Dunkel, S. Heidenreich, K. Drescher, R. E. Goldstein, H. Löwen, and J. M. Yeomans, Mesoscale turbulence in living fluids, Proc. Natl. Acad. Sci. U.S.A. **109**, 14308 (2012).
[11] J. Dunkel, S. Heidenreich, K. Drescher, H. H. Wensink, M. Bär, and R. E. Goldstein, Fluid Dynamics of Bacterial Turbulence, Phys. Rev. Lett. **110**, 228102 (2013).
[12] Y. Peng, Z. Liu, and X. Cheng, Imaging the emergence of bacterial turbulence: Phase diagram and transition kinetics, Sci. Adv. **7**, eabd1240 (2021).
[13] S. J. Ebbens and D. A. Gregory, Catalytic janus colloids: controlling trajectories of chemical microswimmers, Acc. Chem. Res. **51**, 1931 (2018).
[14] I. Theurkauff, C. Cottin-Bizonne, J. Palacci, C. Ybert, and L. Bocquet, Dynamic Clustering in Active Colloidal Suspensions with Chemical Signaling, Phys. Rev. Lett. **108**, 268303 (2012).
[15] F. Ginot, I. Theurkauff, F. Detcheverry, C. Ybert, and C. Cottin-Bizonne, Aggregation-fragmentation and individual dynamics of active clusters, Nat. Commun. **9**, 696 (2018).
[16] L. Baraban, M. Tasinkevych, M. N. Popescu, S. Sanchez, S. Dietrich, and O. Schmidt, Transport of cargo by catalytic janus micro-motors, Soft Matter **8**, 48 (2012).
[17] A. M. Boymelgreen, T. Balli, T. Miloh, and G. Yossifon, Active colloids as mobile microelectrodes for unified label-free selective cargo transport, Nat. Commun. **9**, 760 (2018).
[18] P. Mena-Giraldo and J. Orozco, Polymeric micro/nanocarriers and motors for cargo transport and phototriggered delivery, Polymers **13**, 3920 (2021).
[19] A.-I. Bunea and R. Taboryski, Recent advances in microswimmers for biomedical applications, Micromachines **11**, 1048 (2020).
[20] S. K. Srivastava, M. Medina-Sánchez, B. Koch, and O. G. Schmidt, Medibots: Dual-action biogenic microdaggers for single-cell surgery and drug release, Adv. Mater. **28**, 832 (2016).
[21] A. V. Singh, M. H. D. Ansari, C. B. Dayan, J. Giltinan, S. Wang, Y. Yu, V. Kishore, P. Laux, A. Luch, and M. Sitti, Multifunctional magnetic hairbot for untethered osteogenesis, ultrasound contrast imaging and drug delivery, Biomaterials **219**, 119394 (2019).
[22] T. Bhuyan, A. K. Singh, D. Dutta, A. Unal, S. S. Ghosh, and D. Bandyopadhyay, Magnetic field guided chemotaxis of imushbots for targeted anticancer therapeutics, ACS Biomater. Sci. Eng. **3**, 1627 (2017).
[23] M. Medina-Sánchez, L. Schwarz, A. K. Meyer, F. Hebenstreit, and O. G. Schmidt, Cellular cargo delivery: Toward assisted fertilization by sperm-carrying micromotors, Nano Lett. **16**, 555 (2016).
[24] B. J. Nelson, I. K. Kaliakatsos, and J. J. Abbott, Microrobots for minimally invasive medicine, Annu. Rev. Biomed. Eng. **12**, 55 (2010).
[25] A.-I. Bunea and J. Glückstad, Strategies for optical trapping in biological samples: Aiming at microrobotic surgeons, Laser Photonics Rev. **13**, 1800227 (2019).
[26] P. A. York, R. Peña, D. Kent, and R. J. Wood, Microrobotic laser steering for minimally invasive surgery, Sci. Robot. **6**, eabd5476 (2021).
[27] A. A. Evans, T. Ishikawa, T. Yamaguchi, and E. Lauga, Orientational order in concentrated suspensions of spherical microswimmers, Phys. Fluids **23**, 111702 (2011).
[28] F. Alarcón and I. Pagonabarraga, Spontaneous aggregation and global polar ordering in squirmer suspensions, J. Mol. Liq. **185**, 56 (2013).
[29] N. Yoshinaga and T. B. Liverpool, Hydrodynamic interactions in dense active suspensions: From polar order to dynamical clusters, Phys. Rev. E **96**, 020603(R) (2017).

[30] N. Yoshinaga and T. B. Liverpool, From hydrodynamic lubrication to many-body interactions in dense suspensions of active swimmers, Eur. Phys. J. E **41**, 76 (2018).
[31] B. Delmotte, E. E. Keaveny, F. Plouraboué, and E. Climent, Large-scale simulation of steady and time-dependent active suspensions with the force-coupling method, J. Comput. Phys. **302**, 524 (2015).
[32] M. Theers, E. Westphal, K. Qi, R. G. Winkler, and G. Gompper, Clustering of microswimmers: Interplay of shape and hydrodynamics, Soft Matter **14**, 8590 (2018).
[33] N. Oyama, J. J. Molina, and R. Yamamoto, Do hydrodynamically assisted binary collisions lead to orientational ordering of microswimmers?, Eur. Phys. J. E **40**, 95 (2017).
[34] D. Bray, *Cell Movements: From Molecules to Motility*, in Fluid-Structure Interactions in Low-Reynolds-Number Flows, edited by C. Duprat and H. Stone (Garland Science, New York, 2000), 10.1039/9781782628491.
[35] H. S. Jennings, On the significance of the spiral swimming of organisms, Am. Nat. **35**, 369 (1901).
[36] G. Jékely, J. Colombelli, H. Hausen, K. Guy, E. Stelzer, F. Nédélec, and D. Arendt, Mechanism of phototaxis in marine zooplankton, Nature (London) **456**, 395 (2008).
[37] T. Fenchel and N. Blackburn, Motile chemosensory behaviour of phagotrophic protists: Mechanisms for and efficiency in congregating at food patches, Protistologica **150**, 325 (1999).
[38] M. McHenry and J. Strother, The kinematics of phototaxis in larvae of the ascidian aplidium constellatum, Marine Biol. **142**, 173 (2003).
[39] A. Marumo, M. Yamagishi, and J. Yajima, Three-dimensional tracking of the ciliate tetrahymena reveals the mechanism of ciliary stroke-driven helical swimming, Commun. Biol. **4**, 1 (2021).
[40] G. Corkidi, B. Taboada, C. Wood, A. Guerrero, and A. Darszon, Tracking sperm in three-dimensions, Biochem. Biophys. Res. Commun. **373**, 125 (2008).
[41] J. F. Jikeli, L. Alvarez, B. M. Friedrich, L. G. Wilson, R. Pascal, R. Colin, M. Pichlo, A. Rennhack, C. Brenker, and U. B. Kaupp, Sperm navigation along helical paths in 3d chemoattractant landscapes, Nat. Commun. **6**, 7985 (2015).
[42] R. Thar and T. Fenchel, True chemotaxis in oxygen gradients of the sulfur-oxidizing bacterium thiovulum majus, Appl. Environ. Microbiol. **67**, 3299 (2001).
[43] T.-W. Su, I. Choi, J. Feng, K. Huang, E. McLeod, and A. Ozcan, Sperm trajectories form chiral ribbons, Sci. Rep. **3**, 1 (2013).
[44] D. R. Brumley, M. Polin, T. J. Pedley, and R. E. Goldstein, Hydrodynamic Synchronization and Metachronal Waves on the Surface of the Colonial Alga Volvox Carteri, Phys. Rev. Lett. **109**, 268102 (2012).
[45] D. Vilela, M. M. Stanton, J. Parmar, and S. Sánchez, Microbots decorated with silver nanoparticles kill bacteria in aqueous media, ACS Appl. Mater. Interfaces **9**, 22093 (2017).
[46] F. Lancia, T. Yamamoto, A. Ryabchun, T. Yamaguchi, M. Sano, and N. Katsonis, Reorientation behavior in the helical motility of light-responsive spiral droplets, Nat. Commun. **10**, 1 (2019).
[47] A. T. Brown and W. C. K. Poon, Ionic effects in self-propelled Pt-coated Janus swimmers, Soft Matter **10**, 4016 (2014).
[48] A. I. Campbell, R. Wittkowski, B. Ten Hagen, H. Löwen, and S. J. Ebbens, Helical paths, gravitaxis, and separation phenomena for mass-anisotropic self-propelling colloids: Experiment versus theory, J. Chem. Phys. **147**, 084905 (2017).
[49] J. Blake and A. Chwang, Fundamental singularities of viscous flow, J. Eng. Math. **8**, 23 (1974).
[50] C. Pozrikidis, *Boundary Integral and Singularity Methods for Linearized Viscous Flow*, (Cambridge University Press, Cambridge, 1992).
[51] O. S. Pak, E. Lauga, C. Duprat, and H. Stone, Theoretical models of low-reynolds-number locomotion, *Fluid-Structure Interactions in Low-Reynolds-Number Flows* (2015).
[52] E. Lauga and T. R. Powers, The hydrodynamics of swimming microorganisms, Rep. Prog. Phys. **72**, 096601 (2009).
[53] S. Fürthauer, M. Strempel, S. W. Grill, and F. Jülicher, Active chiral fluids, Eur. Phys. J. E **35**, 89 (2012).
[54] B. M. Friedrich and F. Jülicher, Steering Chiral Swimmers Along Noisy Helical Paths, Phys. Rev. Lett. **103**, 068102 (2009).
[55] R. Singh and R. Adhikari, Generalized stokes laws for active colloids and their applications, J. Phys. Commun. **2**, 025025 (2018).
[56] H. Löwen, Chirality in microswimmer motion: From circle swimmers to active turbulence, Eur. Phys. J. Spec. Top. **225**, 2319 (2016).
[57] B. Liebchen and D. Levis, Collective Behavior of Chiral Active Matter: Pattern Formation and Enhanced Flocking, Phys. Rev. Lett. **119**, 058002 (2017).
[58] D. Levis and B. Liebchen, Simultaneous phase separation and pattern formation in chiral active mixtures, Phys. Rev. E **100**, 012406 (2019).
[59] G.-J. Liao and S. H. Klapp, Clustering and phase separation of circle swimmers dispersed in a monolayer, Soft Matter **14**, 7873 (2018).
[60] D. Levis and B. Liebchen, Micro-flock patterns and macro-clusters in chiral active brownian disks, J. Phys. Condens. Matter **30**, 084001 (2018).
[61] J. Bickmann, S. Bröker, J. Jeggle, and R. Wittkowski, Analytical approach to chiral active systems: Suppressed phase separation of interacting Brownian circle swimmers, J. Chem. Phys. **156**, 194904 (2022).
[62] Q.-L. Lei, M. P. Ciamarra, and R. Ni, Nonequilibrium strongly hyperuniform fluids of circle active particles with large local density fluctuations, Sci. Adv. **5**, eaau7423 (2019).
[63] Z. Ma and R. Ni, Dynamical clustering interrupts motility-induced phase separation in chiral active Brownian particles, J. Chem. Phys. **156**, 021102 (2022).
[64] G.-J. Liao and S. H. Klapp, Emergent vortices and phase separation in systems of chiral active particles with dipolar interactions, Soft Matter **17**, 6833 (2021).
[65] B. Liebchen and D. Levis, Chiral active matter, Europhys. Lett. **139**, 67001 (2022).

[66] D. Levis, I. Pagonabarraga, and B. Liebchen, Activity induced synchronization: Mutual flocking and chiral self-sorting, Phys. Rev. Res. **1**, 023026 (2019).
[67] F. Fadda, J. J. Molina, and R. Yamamoto, Dynamics of a chiral swimmer sedimenting on a flat plate, Phys. Rev. E **101**, 052608 (2020).
[68] P. S. Burada, R. Maity, and F. Jülicher, Hydrodynamics of chiral squirmers, Phys. Rev. E **105**, 024603 (2022).
[69] R. Maity and P. Burada, Near and far-field hydrodynamic interaction of two chiral squirmers, Phys. Rev. E **106**, 054613 (2022).
[70] R. Maity and P. Burada, Unsteady chiral swimmer in presence of an external chemical gradient, J. Fluid Mech. **940**, A13 (2022).
[71] S. Rode, J. Elgeti, and G. Gompper, Multi-ciliated microswimmers–metachronal coordination and helical swimming, Eur. Phys. J. E **44**, 76 (2021).
[72] M. Lisicki, S. Y. Reigh, and E. Lauga, Autophoretic motion in three dimensions, Soft Matter **14**, 3304 (2018).
[73] C. Chen, S. Liu, X.-q. Shi, H. Chaté, and Y. Wu, Weak synchronization and large-scale collective oscillation in dense bacterial suspensions, Nature (London) **542**, 210 (2017).
[74] B. Zhang, B. Hilton, C. Short, A. Souslov, and A. Snezhko, Oscillatory chiral flows in confined active fluids with obstacles, Phys. Rev. Res. **2**, 043225 (2020).
[75] V. B. Putz and J. M. Yeomans, Hydrodynamic synchronisation of model microswimmers, J. Stat. Phys. **137**, 1001 (2009).
[76] B. Qian, H. Jiang, D. A. Gagnon, K. S. Breuer, and T. R. Powers, Minimal model for synchronization induced by hydrodynamic interactions, Phys. Rev. E **80**, 061919 (2009).
[77] N. Uchida and R. Golestanian, Synchronization and Collective Dynamics in a Carpet of Microfluidic Rotors, Phys. Rev. Lett. **104**, 178103 (2010).
[78] J. Kotar, M. Leoni, B. Bassetti, M. C. Lagomarsino, and P. Cicuta, Hydrodynamic synchronization of colloidal oscillators, Proc. Natl. Acad. Sci. U.S.A. **107**, 7669 (2010).
[79] R. Golestanian, J. M. Yeomans, and N. Uchida, Hydrodynamic synchronization at low Reynolds number, Soft Matter **7**, 3074 (2011).
[80] M. Theers and R. G. Winkler, Synchronization of rigid microrotors by time-dependent hydrodynamic interactions, Phys. Rev. E **88**, 023012 (2013).
[81] K. Han, G. Kokot, S. Das, R. G. Winkler, G. Gompper, and A. Snezhko, Reconfigurable structure and tunable transport in synchronized active spinner materials, Sci. Adv. **6**, eaaz8535 (2020).
[82] O. S. Pak and E. Lauga, Generalized squirming motion of a sphere, J. Eng. Math. **88**, 1 (2014).
[83] M. Lighthill, On the squirming motion of nearly spherical deformable bodies through liquids at very small Reynolds numbers, Commun. Pure Appl. Math. **5**, 109 (1952).
[84] J. R. Blake, A spherical envelope approach to ciliary propulsion, J. Fluid Mech. **46**, 199 (1971).
[85] See Supplemental Material at http://link.aps.org/supplemental/10.1103/PhysRevLett.130.024001 for additional details for the surface slip-flow, computational details, and mapping to SI units. It includes additional Refs. [89–104].
[86] B. Zhang, A. Sokolov, and A. Snezhko, Reconfigurable emergent patterns in active chiral fluids, Nat. Commun. **11**, 1 (2020).
[87] K. Drescher, K. C. Leptos, I. Tuval, T. Ishikawa, T. J. Pedley, and R. E. Goldstein, Dancing Volvox: Hydrodynamic Bound States of Swimming Algae, Phys. Rev. Lett. **102**, 168101 (2009).
[88] A. Bricard, J.-B. Caussin, N. Desreumaux, O. Dauchot, and D. Bartolo, Emergence of macroscopic directed motion in populations of motile colloids, Nature (London) **503**, 95 (2013).
[89] J. S. Lintuvuori, A. T. Brown, K. Stratford, and D. Marenduzzo, Hydrodynamic oscillations and variable swimming speed in squirmers close to repulsive walls, Soft Matter **12**, 7959 (2016).
[90] Z. Shen, A. Wrger, and J. S. Lintuvuori, Hydrodynamic interaction of a self-propelling particle with a wall, Eur. Phys. J. E **41**, 39 (2018).
[91] A. J. Ladd, Numerical simulations of particulate suspensions via a discretized Boltzmann equation. part 1. Theoretical foundation, J. Fluid Mech. **271**, 285 (1994).
[92] A. J. Ladd, Numerical simulations of particulate suspensions via a discretized Boltzmann equation. part 2. Numerical results, J. Fluid Mech. **271**, 311 (1994).
[93] N.-Q. Nguyen and A. J. C. Ladd, Lubrication corrections for lattice-Boltzmann simulations of particle suspensions, Phys. Rev. E **66**, 046708 (2002).
[94] I. Llopis and I. Pagonabarraga, Hydrodynamic interactions in squirmer motion: Swimming with a neighbour and close to a wall, J. Non-Newtonian Fluid Mech. **165**, 946 (2010).
[95] I. Pagonabarraga and I. Llopis, The structure and rheology of sheared model swimmer suspensions, Soft Matter **9**, 7174 (2013).
[96] A. Donev, I. Cisse, D. Sachs, E. A. Variano, F. H. Stillinger, R. Connelly, S. Torquato, and P. M. Chaikin, Improving the density of jammed disordered packings using ellipsoids, Science **303**, 990 (2004).
[97] Z. Zhou, R. Zou, D. Pinson, and A. Yu, Discrete modelling of the packing of ellipsoidal particles, AIP Conf. Proc. **1542**, 357 (2013).
[98] B. Martinez-Haya and A. Cuetos, Simulation study of discotic molecules in the vicinity of the isotropic–liquid crystal transition, Mol. Simul. **35**, 1077 (2009).
[99] S. Li, J. Zhao, P. Lu, and Y. Xie, Maximum packing densities of basic 3d objects, Chin. Sci. Bull. **55**, 114 (2010).
[100] L. Liu, Y. Yuan, W. Deng, and S. Li, Evolutions of packing properties of perfect cylinders under densification and crystallization, J. Chem. Phys. **149**, 104503 (2018).
[101] L. Liu, Z. Li, Y. Jiao, and S. Li, Maximally dense random packings of cubes and cuboids via a novel inverse packing method, Soft Matter **13**, 748 (2017).
[102] G. D. Scott and D. M. Kilgour, The density of random close packing of spheres, J. Phys. D **2**, 863 (1969).
[103] J. G. Berryman, Random close packing of hard spheres and disks, Phys. Rev. A **27**, 1053 (1983).
[104] S. Torquato, T. M. Truskett, and P. G. Debenedetti, Is Random Close Packing of Spheres Well Defined?, Phys. Rev. Lett. **84**, 2064 (2000).